A high-resolution wave energy assessment of south-east Australia based on a 40-year hindcast

Jin Liu [a], Alberto Meucci [a], Qingxiang Liu [b,a], Alexander V. Babanin [a], Daniel Ierodiaconou [c], Xingkun Xu [a], Ian R. Young [a,*]

[a] Department of Infrastructure Engineering, University of Melbourne, Melbourne, Victoria, Australia
[b] Physical Oceanography Laboratory, Ocean University of China, Qingdao, China
[c] School of Life and Environmental Sciences, Deakin University, Warrnambool, Victoria, Australia

ARTICLE INFO

ABSTRACT

In this study, a third-generation ocean wave model (WAVEWATCH III; WW3) implemented on a high-resolution unstructured grid was developed to investigate wave energy in the south-east of Australia over the 40-year period from 1981 to 2020. The simulated wave power shows good agreement with values estimated from multiplatform satellite data. Thus, the modeled data were used to study statistics (mean conditions, seasonality, extremes, and long-term trends) of wave power in the domain, which show impacts of Southern Ocean swell and protection provided by the land mass of Tasmania. The results indicate increasing wave power trends, with the largest values in the southeastern part of the domain over the 40-year period. These positive trends are mainly a result of an increase in significant wave height rather than peak wave period. By utilizing the simulated wave properties, we estimated regional annual electric power at 14 coastal locations using 9 typical wave energy converters (WECs). To do so, we conducted a comprehensive analysis (seasonal variations, wave power roses, probability distributions, and bivariate probability distributions) at these locations. The results demonstrate that the western and southwestern coasts of the domain are promising generation sites but with large seasonal variability. The central and eastern coasts are protected by Tasmania, and exhibit more stable conditions but are far less energetic for electricity production. This study has critical implications for the region, which provides a benchmark for coastal WEC deployment.

1. Introduction

Sustainable development strategies often focus on renewable energy, which has highlighted potential resources available from ocean surface waves. Unlike wind or solar, ocean waves have less diurnal variability and represent a relatively reliable energy source [1,2]. However, it is difficult to estimate the wave energy resource by the use of in situ observation, as distributions of such measurements are too sparse to obtain a comprehensive understanding of wave energy variations within a domain. Identifying the most promising locations and assessing their energy potential require long-term modelling at high spatial and temporal resolutions. As such regions are usually in coastal locations, the model should be able to adequately capture the influences of the coastal bathymetry, whilst also accurately simulating swells which may arrive from remote generation sources many thousands of kilometers away.

The Australian coastline is subject to a relatively energetic wave climate [3]. This is particularly the case for the southern half of the continent, where the wave climate is dominated by energetic Southern Ocean swells [4,5]. The southern coast of Australia has been suggested as a suitable location for the deployment of wave energy converters (WECs) for electricity generation [6]. However, a detailed analysis of the wave power climate in the region is a prerequisite for future WEC deployment. Moreover, the south-east coast (Fig. 1a) is one of the most densely populated regions in Australia. Therefore, understanding wave power variation in this region is beneficial in serving the local community, reducing greenhouse gas emissions, and building a sustainable environment.

There are only a limited number of wave energy assessments which have been conducted on either national or regional scales for Australia. Using a 0.1° AusWAM model dataset, Hughes and Heap [6] estimated the mean wave power (i.e., wave energy flux) for each Australian state and found wave power on the southern Australian shelf is promising for

---

WEC developments. Based on multiple nesting of the SWAN model, Cuttler et al. [7] evaluated the wave conditions and wave power variation near Albany, Western Australia, which is a targeted location for future WEC installation. Morim et al. [8] reported that the central coast of New South Wales is a very promising region in eastern Australia for wave power exploitation. They also discussed wave power characteristics at selected locations. Based on a geographic information system (GIS) approach, Flocard et al. [9] demonstrated that western Victoria is a promising area for wave power extraction. This analysis considered different physical, environmental, and socioeconomic indices to identify regions with suitable characteristics for WEC exploration. However, their study did not conduct detailed wave power analysis at selected locations nor estimate the potential electric power of WECs.

There are numerous wave power assessments conducted in various ocean regions worldwide. However, southeastern Australia stands out as a particularly interesting area that warrants a comprehensive investigation of wave power, given its unique complexity. This region is exposed to the powerful swells of the Southern Ocean, while eastern Victoria is influenced by prevailing eastern winds. Additionally, the bathymetry of the area is notably complex, with the presence of Bass Strait and Tasmania. Consequently, southeastern Australia serves as an ideal domain for exploring the feasibility of wave power extraction.

In this paper, a high-resolution wave hindcast model was adopted to investigate wave power distribution and variability over the period 1981–2020 in south-east Australia. A total of 14 locations, along the coast of Victoria, Tasmania, eastern South Australia, and southern New South Wales, were selected to conduct detailed wave power analysis. The paper is organized as follows. Section 2 introduces the data and methodology used. Section 3 validates the wave model against satellite altimeter data and derived wave power. Section 4 describes the wave power climatology of the domain and the wave power variability and expected electricity production at the selected sites, followed by brief conclusions in Section 5.

2. Data and methods

2.1. Satellite-derived wave power

Satellite altimeters provide long-term global monitoring of sea state [11,12]. Ribal and Young [12] calibrated and validated global multi-mission altimeter significant wave height (H_s) and wind speed (U_{10}) against National Oceanographic Data Center (NODC) buoys. This satellite dataset covers 14 altimeters from 1985 to 2020 (SENTINEL-3B was added recently, Fig. 2), and can be accessed through the Australian Ocean Data Network (AODN) portal (https://portal.aodn.org.au).

The following analysis is largely based on the wave energy flux, $C_g E = \rho g \overline{C_g} E$ [kW/m] evaluated internally by the WAVEWATCH III model (WW3) [13]. Here, ρ is the density of seawater, g is gravitational acceleration, $\overline{C_g}$ is the mean value of wave group velocity and $E = \int$

$F(f,\theta)\, df d\theta$ is the total energy of the spectrum, $F(f,\theta)$, where f is frequency and θ is direction. Consistent with previous literature [14], we will refer to this quantity as wave power. This should not be confused with the electrical power produced by a wave energy converter, which has units of [MWh].

The wave power ($C_g E$) cannot be directly measured by satellite altimeters, which provide values of the significant wave height, H_s, wind speed, U_{10} and radar cross-section, σ_0. However, it can be inferred from H_s and energy period (T_e), which for deep water are related by [14–17],

$$C_g E \approx \frac{\rho g^2}{64\pi} T_e H_S^2, \tag{1}$$

where T_e can be approximated from the peak wave period, T_p by

$$T_e = \alpha T_P, \tag{2}$$

where a range of values (0.5–0.9) have been proposed for the coefficient α [9,14,16,18–21], depending on the shape of the wave spectrum. Here, we choose $\alpha = 0.7$ for the present domain, which is consistent with previous studies and measurements along the Victorian coast of Australia by Flocard et al. [9]. Although the choice of this parameter could introduce some uncertainty in the estimation of wave power [19], the impact tends not to be large compared to errors in estimated H_s, as wave power is proportional to H_s^2 [22]. Following Gommenginger et al. [23], the peak wave period (T_p) can be calculated by,

$$\log_{10}(T_p) = 0.154 + 1.797 \times \log_{10}(X), \tag{3}$$

where $X = (\sigma_0 \times H_{SKu}^2)^{0.25}$, where σ_0 is the Ku-band radar backscatter coefficient [dB], H_{sKu} is the Ku-band H_s [m]. Ribal et al. [14] reported that σ_0 in Eq. (3) can also be used for Ka-band radar backscatter, as in the case of the SARAL altimeter.

2.2. Ocean wave model

The third-generation ocean wave model [13], WAVEWATCH III (WW3, version 6.07), was developed from its earlier versions, WW1 and WW2 [24,25]. The WW3 model is a community-driven framework representing present day understanding of the evolution of the directional wave spectrum. The WW3 model solves the wave action density balance equation [13],

$$\frac{dN}{dt} = \frac{S_{tot}}{\omega}, \tag{4}$$

where $N = F/\omega$ is wave action spectrum, t is time, $\omega = 2\pi f$ is the angular frequency, S_{tot} is the total source/sink term which includes linear wind input S_{ln} at the initial stages of wave growth, wind input S_{in}, white-cap dissipation S_{wc}, swell dissipation S_{sw}, nonlinear interactions S_{nl}, bottom friction S_{bot} and depth-induced wave breaking S_{db}.
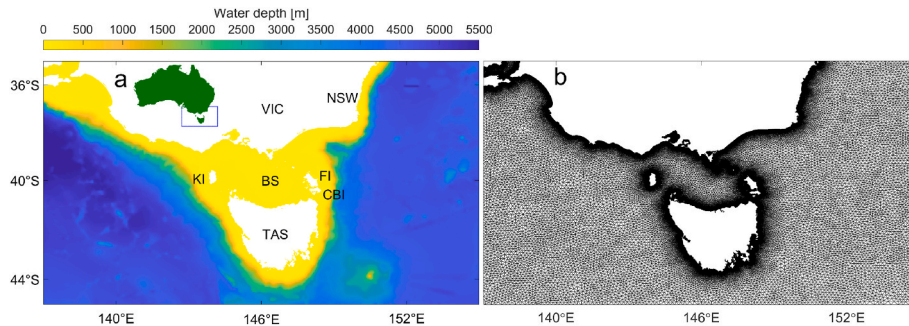

Fig. 1. (a) Water depth and (b) the unstructured grid of the model domain [10]. The insert is Australia. The blue line in the insert denotes where open boundary wave spectra data were provided by the global wave hindcast model. The domain covers South Australia (SA), Victoria (VIC), New South Wales (NSW), Tasmania (TAS), King Island (KI), Flinders Island (FI), Cape Barren Island (CBI), and Bass Strait (BS).
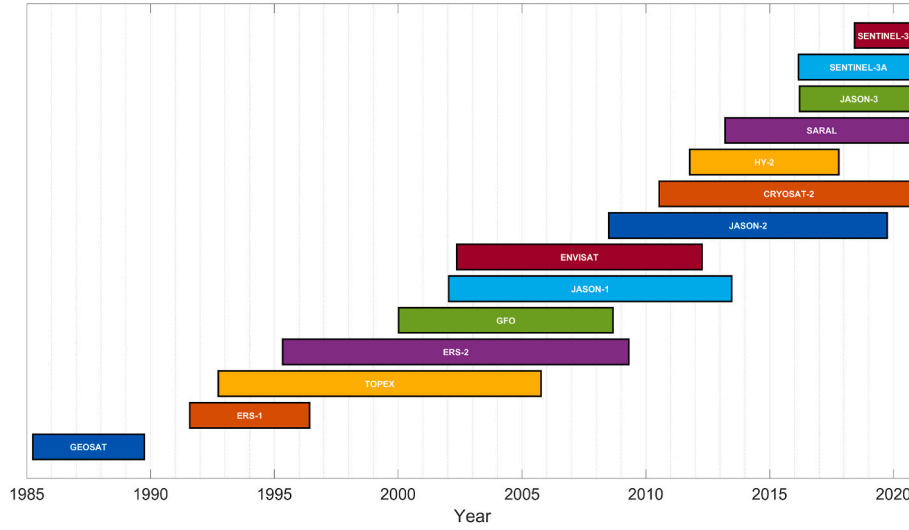
Fig. 2. Duration of satellite altimeter missions over the period 1985–2020.

$$S_{tot} = S_{ln} + S_{in} + S_{wc} + S_{sw} + S_{nl} + S_{bot} + S_{db}, \tag{5}$$

The linear input source term was defined by Cavaleri and Rizzoli [26], with energy filtering represented by Tolman [25]. The nonlinear quadruplet wave-wave interactions were represented by the discrete interaction approximation approach proposed by Hasselmann et al. [27], which are of significance when simulating ocean waves, especially during extreme wave conditions [28]. JONSWAP bottom friction was implemented as parameterized by Hasselmann et al. [29]. The depth-induced wave breaking term used the formulation of Battjes and Janssen [30]. The wind input, white cap dissipation, and swell dissipation were implemented through the ST6 wave package [31,32]. Default values were used for all parameter settings unless otherwise specified.

Water depth is an important factor in defining wave characteristics in nearshore regions. In this study, the near-shore bathymetric data were obtained from the Victorian Coastal Digital Elevation Model, which can be downloaded from the AODN. The offshore bathymetric data were sourced from the Australian Bureau of Meteorology (BOM, http://www.bom.gov.au). Based on the bathymetric characteristics in the domain (Fig. 1a), an unstructured model grid (Fig. 1b) was generated through the approach proposed by Roberts et al. [33].

Ocean waves in coastal regions undergo significant changes due to variations in water depth. As a result, a high-resolution model grid is necessary in these areas. The WW3 model offers the flexibility to utilize both structured and unstructured grids in order to achieve this objective [13]. One approach involves nesting models of different scales within a structured grid, although this typically demands substantial computing resources. On the other hand, an unstructured grid with high resolution in coastal regions [20,21,34] and relatively lower resolution in offshore areas can effectively capture coastal features while maintaining computational efficiency.

Hourly ERA5 reanalysis winds [35] on an 0.25°grid from the European Centre for Medium-Range Weather Forecasts (ECMWF) were used to force the WW3 model. The ERA5 data covers the period from 1950 to the present and can be accessed from https://cds.climate.copernicus.eu. The spectral data on the open boundary (the blue line in Fig. 1a) were sourced from the global wave hindcast model of Liu et al. [36], which used the same ERA5 winds and wave physics as the present regional model.

The WW3 model was discretized using 36 directions (0–360°) and 35 frequencies (0.037–0.953 Hz). It was run for the period from 1981 to 2020 with a time step of 20 min. Values of H_s, T_p, and C_gE were archived every hour. As noted above, wave power is represented by C_gE [14].

Following Kaur et al. [37], an empirical proportional method was applied to Eq. (1) to estimate the percentage contributions of significant wave height (P_{H_s} [%]) and peak wave period (P_{T_p} [%]) to wave power.

$$P_{H_s} = \frac{H_s^2}{H_s^2 + T_p} \times 100\%, \tag{6}$$

$$P_{T_p} = \frac{T_p}{H_s^2 + T_p} \times 100\%, \tag{7}$$

where H_s has units of [m] and T_p has units of [s].

2.3. Model skill metrics

There are many metrics that can be used to describe model performance. Here, the following commonly used metrics were selected to quantify model skill, namely Pearson's correlation coefficient (CC), root mean square error (RMSE), scatter index (SI), and bias value (Bias).

$$CC = \frac{\sum_{i=1}^{N}(O_i - \overline{O_i})(S_i - \overline{S_i})}{\sqrt{\sum_{i=1}^{N}(O_i - \overline{O_i})^2 \sum_{i=1}^{N}(S_i - \overline{S_i})^2}}, \tag{8}$$

$$RMSE = \sqrt{\frac{1}{N}\sum_{i=1}^{N}(S_i - O_i)^2}, \tag{9}$$

$$SI = \frac{RMSE}{\overline{O}}, \tag{10}$$

$$Bias = \overline{S} - \overline{O}, \tag{11}$$

where S and O represent values of model and observations, respectively. Overlines for S and O represent the corresponding mean values.

3. Model validation

Liu et al. [10] have extensively validated the model wave parameters (significant wave height, peak wave period/direction) against a coastal buoy network. In this study, we further validate the model outputs against a multi-platform satellite altimeter dataset. As we are using a high-resolution unstructured grid, it is possible to co-locate each altimeter 1-Hz record with the nearest model node with minimal error (i. e., mesh size is often smaller than the altimeter along-track resolution).
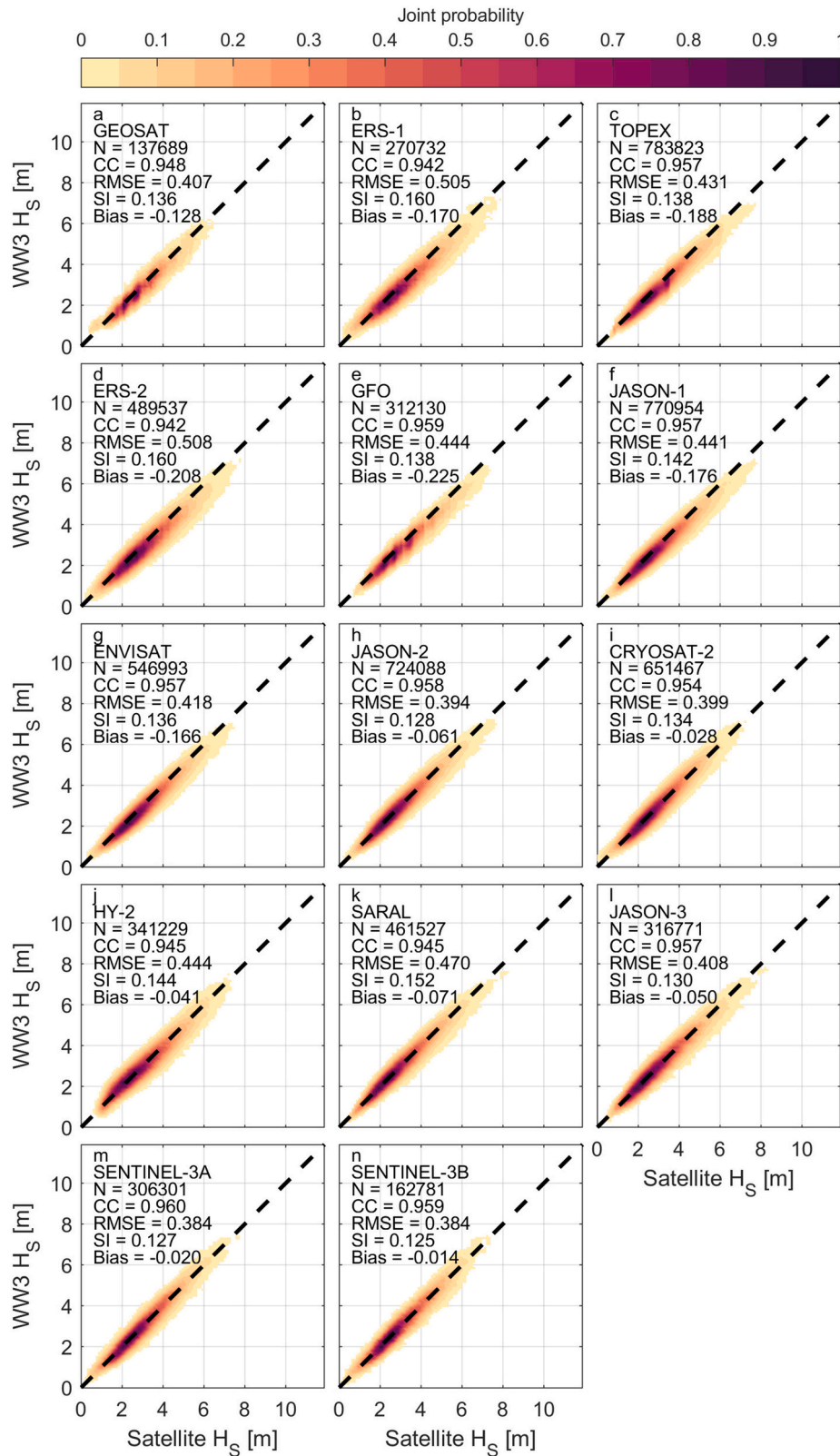
Fig. 3. Comparisons of significant wave height between the WW3 hindcast and satellite altimeters. The satellite name, number of observations (*N*), correlation coefficient (*CC*), root mean square error (*RMSE*), scatter index (*SI*) and bias value (*Bias*) are shown in each panel.

Fig. 3 shows density plots of co-located significant wave height from the WW3 model and each satellite altimeter. The results show the model is slightly biased low compared to the observations across all altimeters, which is a result of underestimated wind speed in the coastal regions of eastern Victoria [10]. Moreover, as the altimeters were launched by different agencies and the altimetry technology is constantly developing, the model skill metrics vary slightly. All the results in Fig. 3, however, show good agreement between the simulated and observed

significant wave height with the comparisons closely aligning with the 1:1 line. The model skill metrics are also very promising and comparable with previous comparisons between wave model and altimeter observations in other regions (e.g., Indonesia [14] and China's adjacent seas [17,22]).

Satellite altimeters cannot measure wave power directly, however,

this quantity can be approximated from Eqs. (1)–(3). Fig. 4 shows the comparisons between modeled and altimeter-inferred wave power. The joint probability (density plot) of wave power in Fig. 4 is more scattered than that of the significant wave height comparisons in Fig. 3. This is because the wave energy period and peak wave period are derived based on empirical functions [14] and wave power is proportional to H_s^2 (Eq.
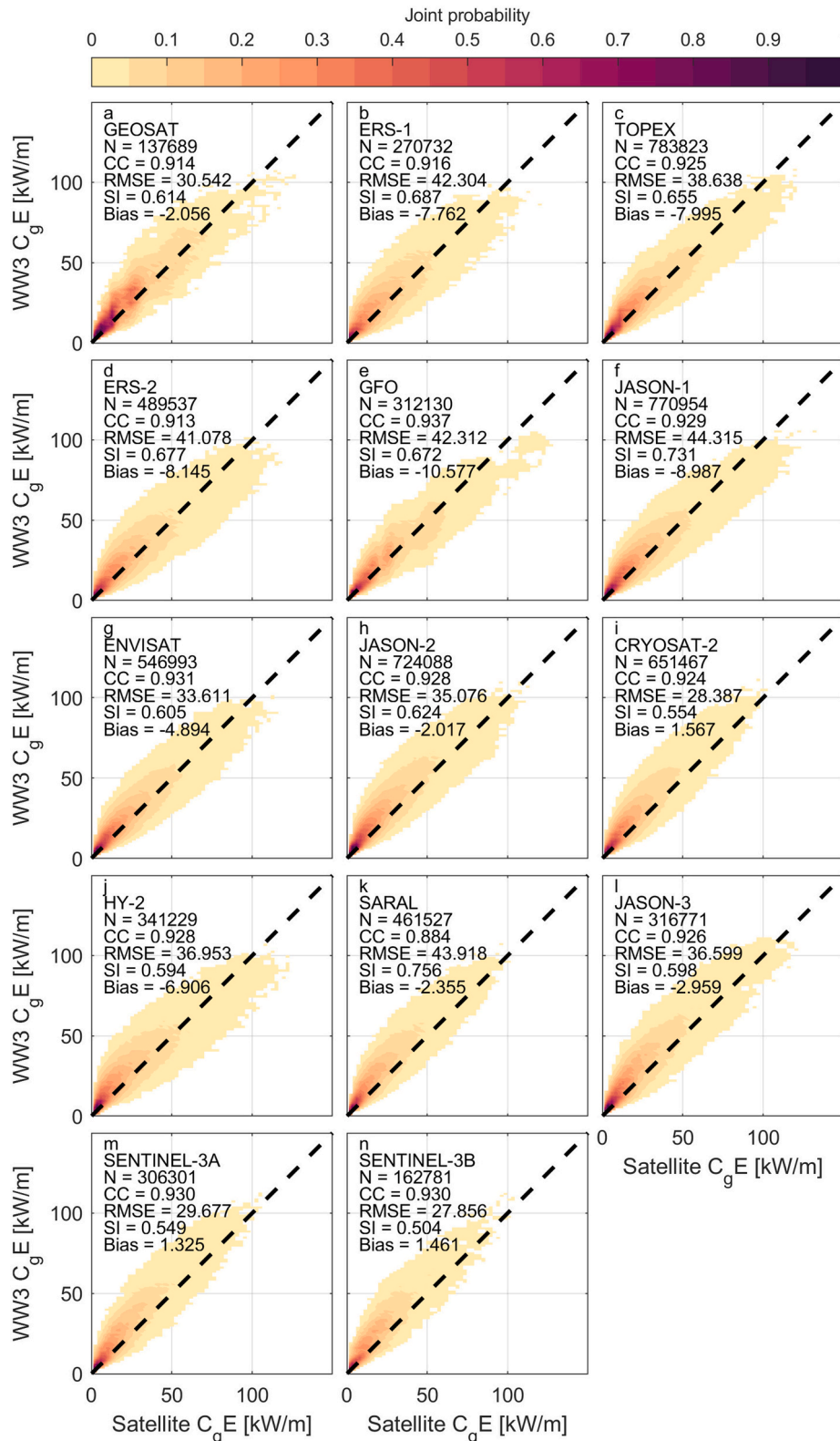

Fig. 4. As for Fig. 3 but for wave power.

(1)). Compared with Ribal et al. [14], the present model skill metrics for wave power show better performance in correlation coefficient and scatter index. However, the root mean square error and bias values are higher than Ribal et al. [14]. The present study, however, considers wave power for south-east Australia (Fig. 1a), which includes both the deep ocean and the coastal regions. In contrast, Ribal et al. [14] only considered wave power in coastal regions. Another difference is that the wave power in the present domain is considerably more energetic and seasonal than Ribal et al. [14]. The results in Figs. 3 and 4 do, however, show that the model can simulate wave power in south-east Australia with reasonable accuracy.

While the comparisons of wave power between the WW3 model and satellite altimeters demonstrate good agreement, it is important to acknowledge the presence of uncertainties. One factor contributing to these uncertainties is the dependence of altimeter-induced wave power on the parameter α in Eq. (2), which is associated with the wave spectrum. The selection of α can impact the calculated altimeter-induced wave power, introducing some variability in the results. Additionally, it is worth noting that the validation of the model results is based on altimeter data with quality flags of "good" or "probably good," primarily obtained from offshore regions [38]. As a result, the validation process, as depicted in Figs. 3 and 4, excludes shallow waters where altimeter data is of questionable quality [11].

4. Results and discussion

Liu et al. [10] reported that the present model shows very good performance in simulating ocean waves in south-east Australia based on validations against coastal buoy observations. Section 3 in this study further verified significant wave height and wave power against multi-platform satellite altimeter data, which also shows good agreement between the model and observations. These results add confidence that the model represents a valid tool for undertaking a detailed analysis of wave power for the region.

4.1. Mean values of wave power

Fig. 5a shows the mean wave power averaged over the period 1981–2020 across the model domain. Not surprisingly, the wave power in the southern and western parts of the domain is very large due to the energetic Southern Ocean swell approaching the region. Bass Strait and the northeastern regions of the domain, however, are protected by Tasmania and thus show much lower wave power. The distributions of significant wave height and peak wave period of Liu et al. [10] show similar spatial distributions as wave power (Fig. 5a). The percentage contribution of the peak wave period to the wave power (Eq. (7), Fig. 5c) can reach 75–90% in regions protected by Tasmania (e.g., Bass Strait and nearshore regions of eastern Victoria). Along the southern and western boundaries with more energetic waves, however, both significant wave height and peak wave period provide similar contributions to the resultant wave power (Fig. 5b and c).

4.2. Seasonality of wave power

The wave power was also averaged over each season for the period 1981–2020 (Fig. 6a–d), with strong seasonality observed. Seasonal wave power in the domain reaches its maximum in winter and minimum in summer, due to the long period energetic Southern Ocean swell approaching the domain in winter. In winter, wave power in the southwestern proportion of the domain can reach approximately 90 kW/m, however, it drops to ~50 kW/m in summer. The percentage contribution of H_s to the seasonal wave power shows similar patterns to the total wave power, with the largest percentage contribution in winter, reducing in summer (Fig. 6e–h). Not surprisingly, the percentage contribution of the seasonal peak wave period is the opposite, with the peak wave period contributing more to the total wave power in summer than winter (Fig. 6i-l).

Long-shore sediment transport was found to be related to wave power [39]. Consequently, it is not surprising that changes in wave power can lead to beach erosion/accretion or beach rotation [40,41]. For instance, the Patterson River in the eastern Port Phillip Bay has undergone noticeable beach rotation as a result of seasonal changes in ocean waves. Additionally, the Victorian Government's Department of Energy, Environment and Climate Action implemented a beach nourishment program to address concerns regarding beach erosion in coastal regions, e.g., Sandringham, Dromana and St Leonards in Port Phillip Bay.

4.3. Temporal variability of wave power

Temporal variability of wave power is an important consideration for WEC deployment. A region with steady moderate wave power may be more suitable to install a WEC device than an energetic but variable area. Here, the annual/seasonal/monthly variability index (*VI*) and coefficient of variation (*COV*) were calculated to quantify the variability of the wave power [15,16,19].

$$VI = \frac{C_gE_{\max} - C_gE_{\min}}{\overline{C_gE}}, \tag{12}$$

$$COV = \frac{\sigma}{\mu}, \tag{13}$$

where C_gE_{max} (C_gE_{min}) is the mean wave power in the most (least) energetic year, season, and month for annual, seasonal, and monthly variability index, respectively. $\overline{C_gE}$ is the yearly mean wave power. The values σ and μ are the standard deviation and mean values of wave power, respectively.

Fig. 7 shows the variability indices based on the different temporal scales and the coefficient of variation of wave power. The spatial distributions show that the western regions of the domain have larger variability amplitude than the eastern parts of the domain. Nearshore regions of northern Tasmania also show high variability. Coastal regions of eastern Victoria and eastern Tasmania, however, have low variability
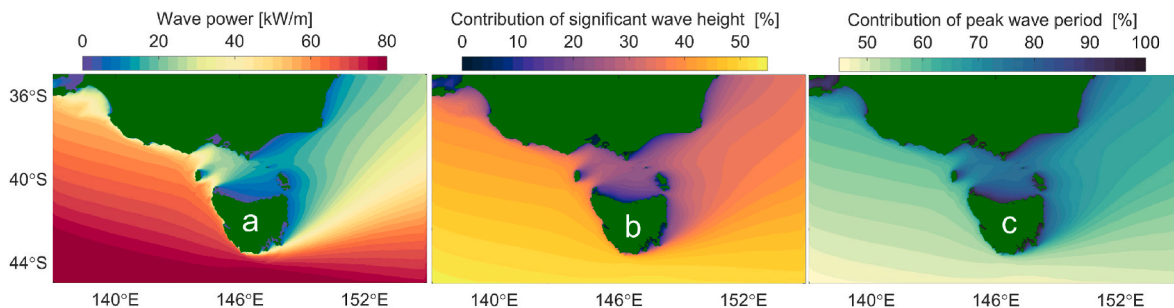
Fig. 5. (a) Mean wave power and the percentage contributions of (b) significant wave height and (c) peak wave period to wave power over the period 1981–2020. Note the different scales of the color bar in (b) and (c).
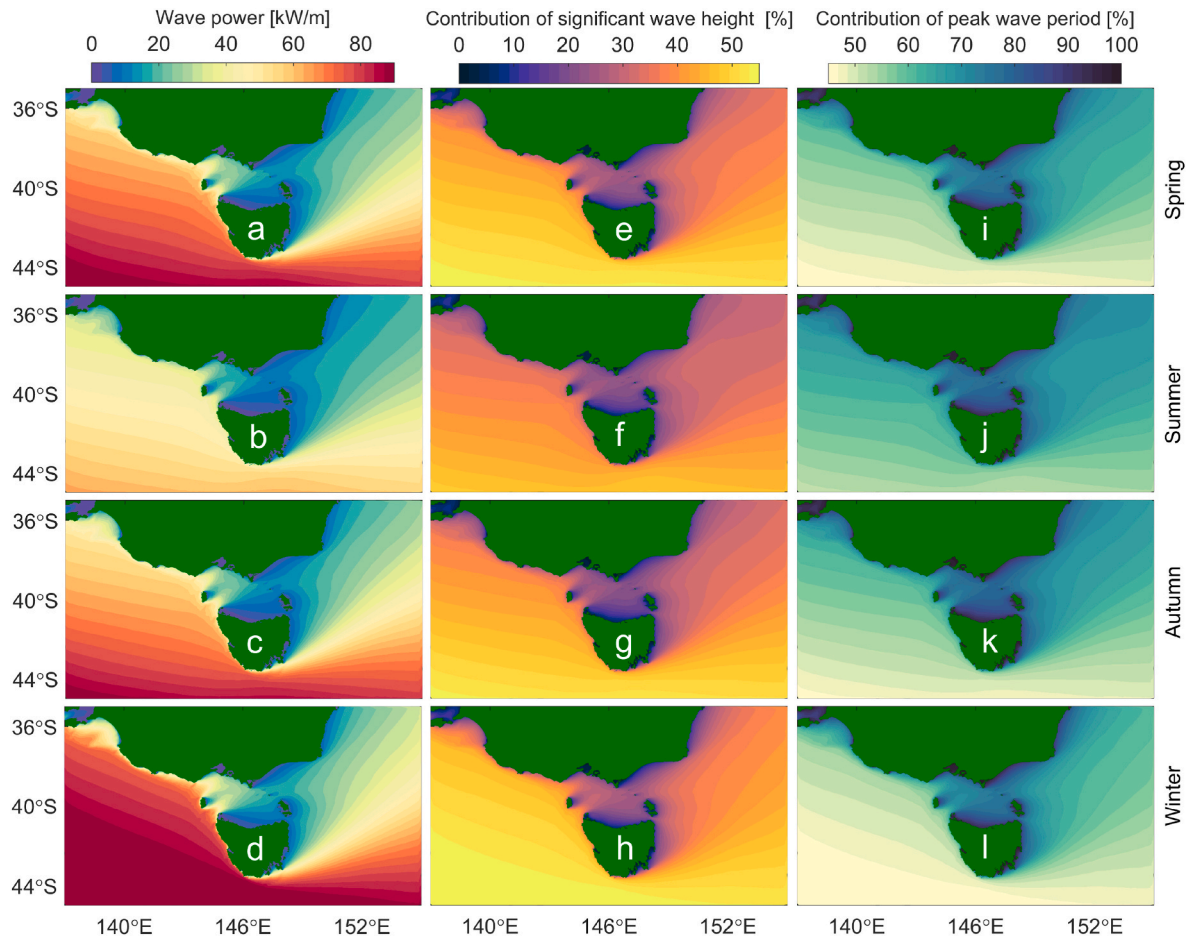
Fig. 6. (a–d) Seasonal wave power and the percentage contributions of (e–h) significant wave height and (i–l) peak wave period to wave power. Austral spring (SON), summer (DJF), autumn (MAM), and winter (JJA). Note the different scales of the color bar in (e–h) and (i–l).
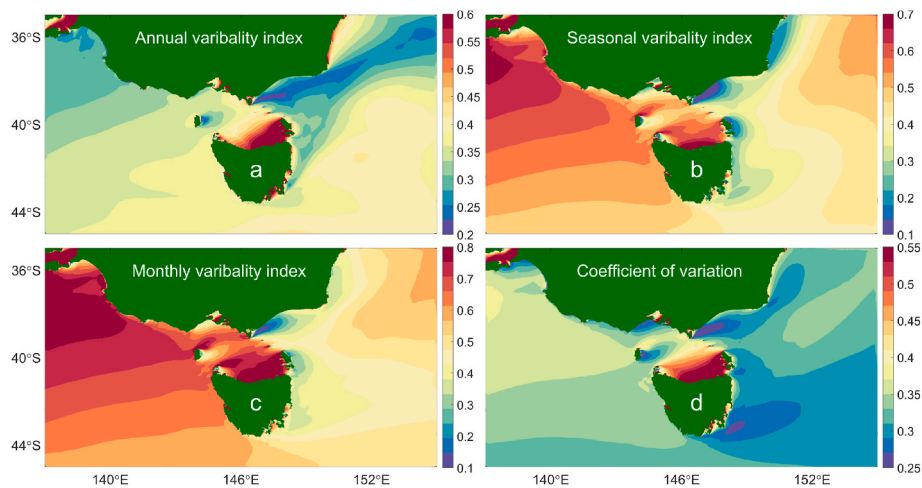

Fig. 7. (a) Annual, (b) seasonal, (c) monthly variability indexes, and (d) coefficient of variation distributions of wave power.

indexes and *COV*.

4.4. Extreme wave power

WECs are often vulnerable to damage during storms. Hence, it is essential to take extreme wave conditions into consideration when placing WECs. Fig. 8 shows distributions of the 90th and 99th percentile wave power. Both percentiles of wave power show large values in the exposed southwestern parts of the domain, whilst the magnitudes in regions protected by Tasmania are much smaller. Such spatial patterns are quite similar to the mean conditions. This means that the extreme wave power is also highly impacted by swell and storm systems from the Southern Ocean as well as the sheltering effects of Tasmania.
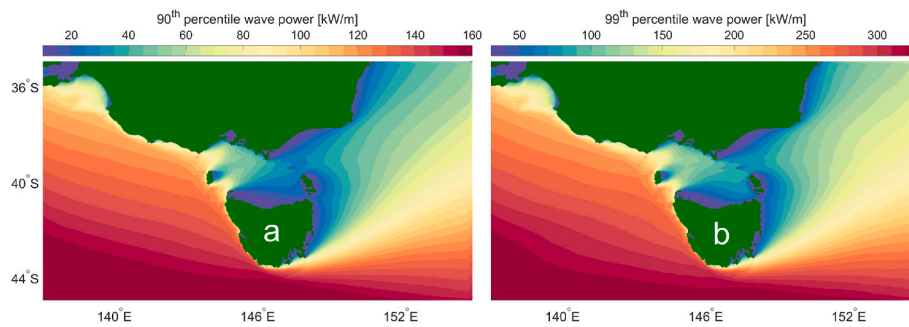
Fig. 8. (a) 90th percentile and (b) 99th percentile wave power.

4.5. Long-term trends of wave power

This study also evaluates long-term variations of wave power in this region based on linear regression of annual wave power (Fig. 9). Fig. 9 shows the percentage change in wave power over the period 1981 to 2020. The results show that most of the domain has increasing trends in wave power over the period. The trends in the southeastern part of the domain show as high as a 14% increase over the period 1981–2020, which is dominated by increases in significant wave height, rather than peak wave period [10]. This can be seen from Fig. 9a in Liu et al. [10], which shows similar spatial distributions of trends for significant wave height as Fig. 9 in the present study. Coastal regions of eastern Victoria, northern and eastern Tasmania, however, show only a small or no increase in wave power (Fig. 9) since changes in both significant wave height and peak wave period are very minor in these areas [10].

It is important to note that the current study did not account for the impacts of ocean currents, mainly due to the unavailability of long-term, high-resolution ocean current data. However, global studies conducted by Rapizo et al. [42] suggest that incorporating current impacts could result in approximately 2% changes in H_s within the study area. This would likely cause slight modifications to wave power.

Furthermore, variations in atmospheric conditions, such as wind patterns, have the potential to influence wind-generated waves in the study area. The Southern Annular Mode (SAM), which impacts the low-pressure systems in the Southern Hemisphere, has shown changes in recent decades [38,43], leading to stronger waves in the Southern Ocean. These changes in wave conditions are expected to have an impact on wave power within the study domain.

Projections of future wave climate under different greenhouse gas emission scenarios can also be investigated for the region. Using the same wave model configuration described above, Liu et al. [44] forced the model with winds from a General Circulation Model (GCM) for different greenhouse gas emission scenarios. They reported that
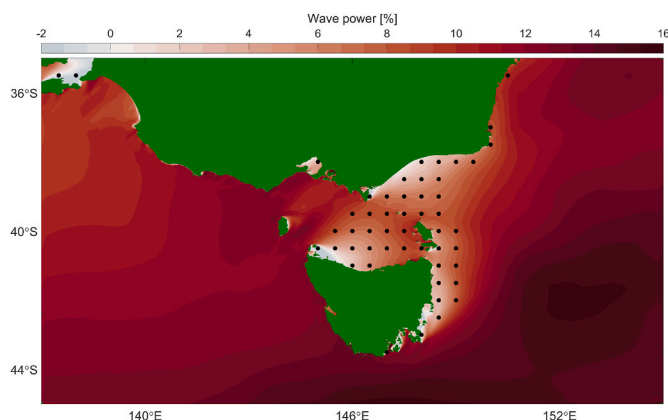

Fig. 9. Percentage change in wave power over the period 1981–2020. Areas statistically significant are marked without dots.

projected values of H_s in the offshore regions of the present domain show a robust increase by the end of the 21st century under a high-emission scenario (SSP5-8.5). However, coastal regions of eastern Victoria show a decrease in H_s due to a projected decrease in local winds. There are, however, few studies of future projections of wave power globally or regionally and no studies have been conducted in the present domain to investigate potential changes in wave power under different scenarios. Future research in this area would be of great value for the deployment of optimal WECs.

4.6. Detailed wave power analysis at selected locations

The installation of WECs generally requires a comprehensive understanding of the local wave climate and estimated wave power. Therefore, it is essential to investigate the detailed characteristics of wave power at targeted locations before installing WEC devices. WECs are generally deployed in nearshore regions. In this study, 14 nearshore locations (Fig. 10) distributed along the coastline were selected for further analysis of wave power. Details of each location are shown in Table 1. The water depths of the locations range from 18 to 100 m and their distances to shore are all less than 4 km. Mean H_s at locations directly exposed to the Southern Ocean (e.g., SA, KI, VIC1-2, TAS1-4) is approximately 1.5–3 times that at locations protected by Tasmania (e.g., VIC4-5, NSW, TAS5-6). The impacts of Tasmania on wave power are much larger than on H_s, as both wave height and period are impacted. For example, wave power at the locations in the western part of the domain is 30–65 kW/m, whereas it is generally below 10 kW/m in nearshore regions of New South Wales, eastern Victoria, and northeastern Tasmania. The temporal variability indices at all locations are smaller than 1 (Table 1), which means these locations are relatively stable in terms of their wave power climate compared with other studies [16,17].

4.6.1. Seasonal wave power at selected locations

Fig. 11 shows annual mean and seasonal wave power at the selected locations. Note the different scales on the y-axis at the locations protected by Tasmania (VIC4-5, NSW, TAS5-6). Seasonal wave power at most of the locations reaches its maximum in winter and minimum in summer. Mean wave power at VIC1-2, KI, and TAS1-3 are large, and their seasonal variabilities are also relatively large. Regions open to the Southern Ocean, show distinct seasonal variations (maximum value minus minimum value) ranging from ~5 kW/m at VIC3 and TAS4 (Fig. 11d, l) to ~37 kW/m at TAS2 (Fig. 11j). VIC4, NSW, and TAS5 are dominated by the local climate system [10] and thus show minimum wave power in spring and maximum in winter (Fig. 11e, g, m). Although wave power values at VIC4 and VIC5 are relatively low, they are seasonally very stable (Fig. 11e and f).

4.6.2. Directional distributions of wave power at selected locations

The directional distribution of wave power is also an important factor when considering WEC setup. Fig. 12 shows wave power roses at
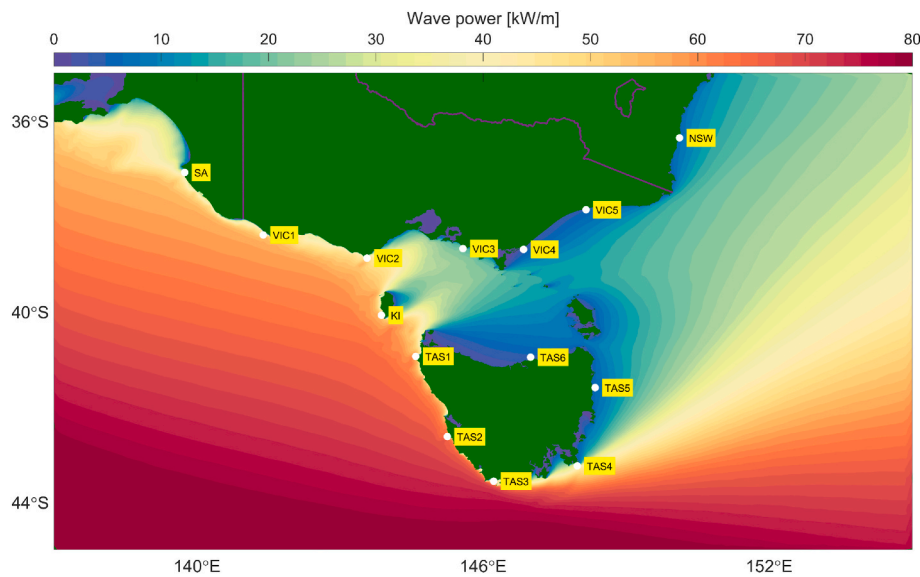
Fig. 10. Selected locations for detailed wave power assessment. The purple lines represent the state borders. The colormap is the annual mean wave power (Fig. 5a). SA=South Australia, VIC=Victoria, NSW=New South Wales, KI=King Island, TAS=Tasmania.

Table 1
Detailed information for selected locations. SA=South Australia, VIC=Victoria, NSW=New South Wales, KI=King Island, TAS=Tasmania. C_gE = wave power. AVI = annual variability index, SVI = seasonal variability index, MVI = monthly variability index, COV = coefficient of variation.

Location	Lon (°E)	Lat (°S)	Depth (m)	Distance to coast (km)	Annual mean H_s (m)	Annual mean C_gE (kW/m)	AVI	SVI	MVI	COV
SA	139.74	37.08	20.39	0.85	2.16	30.88	0.32	0.59	0.74	0.35
VIC1	141.39	38.40	32.10	0.62	2.62	47.19	0.32	0.55	0.69	0.34
VIC2	143.57	38.88	53.98	2.80	2.73	51.81	0.35	0.50	0.64	0.32
VIC3	145.58	38.68	21.23	1.40	1.73	18.31	0.39	0.46	0.63	0.34
VIC4	146.85	38.70	18.78	1.90	0.93	3.50	0.28	0.05	0.15	0.27
VIC5	148.16	37.87	27.12	2.96	0.99	4.56	0.28	0.28	0.40	0.34
NSW	150.12	36.36	45.71	2.42	1.22	6.98	0.50	0.21	0.36	0.37
KI	143.87	40.08	54.57	0.51	2.78	53.24	0.37	0.57	0.71	0.36
TAS1	144.59	40.94	50.23	1.82	2.85	57.08	0.38	0.56	0.70	0.36
TAS2	145.25	42.63	60.79	0.54	3.09	64.42	0.39	0.51	0.62	0.34
TAS3	146.22	43.56	52.33	3.21	2.75	53.39	0.37	0.40	0.52	0.31
TAS4	147.98	43.24	99.41	0.95	2.31	33.31	0.41	0.35	0.43	0.31
TAS5	148.35	41.60	43.44	2.71	1.19	6.33	0.42	0.26	0.38	0.36
TAS6	147.00	40.96	40.98	2.88	0.95	4.23	0.66	0.73	0.97	0.63

the selected locations, discretized into 18 direction bins with a directional step of 20°. The wave power bandwidth is 20 kW/m and the last band includes wave power higher than 80 kW/m. The results indicate that waves at the locations open to the Southern Ocean are very energetic and mainly southwesterly with relatively narrow direction bands (Fig. 12a–d, h-l). This is characteristic of the energetic Southern Ocean swell climate of the region. WECs deployed at these locations should be orientated to the southwest and would not require frequent changes in direction. On the contrary, regions protected by Tasmania have less energetic waves with a broader spread of wave directions (Fig. 12e–g, m, n). The significant wave height is lower and the peak wave period is shorter in these regions than in the southwestern part of the domain. Furthermore, wave directions at these locations show distinct seasonality [10] which results in broad directional distributions. As a result, WECs at these locations would need to be able to accommodate a broad spread of wave directions. These characteristics of narrow directional distributions in the west/southwest and broad directional distributions in the east, are consistent with the wave spectra comparisons at Victorian coastal buoy locations of Liu et al. [10]. While the Southern Ocean swell does have some influence on the wave conditions behind Tasmania, its impact is significantly diminished. On the other hand, local easterly winds prevail in the northeast portion of the domain. The combined effects of these factors result in relatively low wave power

amplitudes (as shown in Fig. 11) and broad wave directions (as depicted in Fig. 12). It is important to note that the northeastern part of the domain is an area where local winds and the Southern Ocean swell interact. Therefore, even slight changes in the Southern Ocean conditions can lead to substantial alterations in wave direction [10].

4.6.3. Wave power probability distributions at selected sites

Fig. 13 shows probability of occurrence distributions and extreme values of wave power at the selected locations. At the locations in the western and southern parts of the domain, wave power is more variable and has a broad probability distribution (Fig. 13a–d, h-l). Approximately 39–62% of the wave power ranges between the values of 10 kW/m to 40 kW/m at these locations. Moreover, extreme wave power at these locations is relatively high, especially at KI and TAS1-3. At the locations protected by Tasmania, more than 80% of the wave power is less than 10 kW/m (Fig. 13e–g, m, n) and the 90th percentile wave power is generally smaller than 15 kW/m. However, a stable wave power distribution does not guarantee efficient power production. For example, wave power below 5 kW/m cannot be efficiently converted by the Pelamis WEC [8].

4.6.4. Electric power production at selected locations

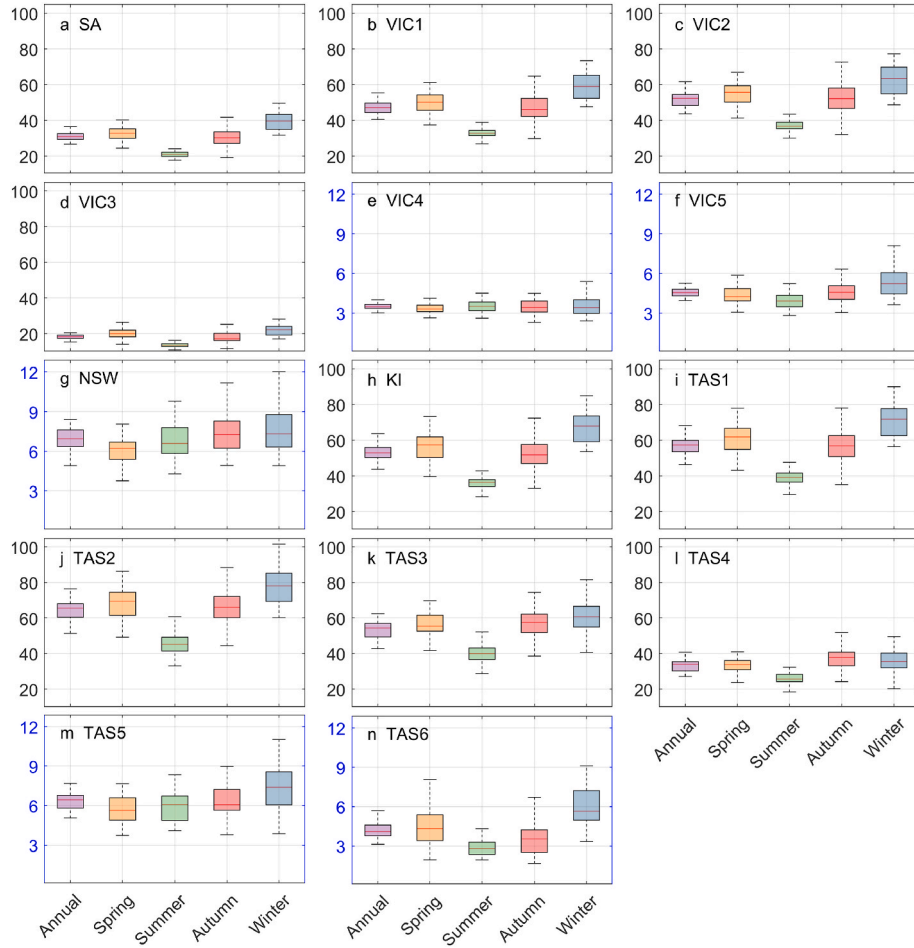Each type of WEC has a specific H_s and T_e range for optimal

Fig. 11. Whisker box plots of annual mean and seasonal wave power (units: kW/m) at selected locations shown in Fig. 10. The middle red line, upper line, and lower line of each box represent the 50th, 75th, and 25th percentile, respectively. The whiskers beyond each box mark the minimum and maximum values. Note the different y-axis scales for regions protected by Tasmania (e-g, m, n).

performance [15]. In order to make an optimal selection of WECs and to understand the wave power capacity at each location, Fig. 14 shows the bivariate probability distribution of occurrence in terms of H_s and T_e and annual wave power storage over 1981–2020. The H_s and T_e values are discretized with steps of 0.25 m and 1 s, respectively. The annual occurrences of each sea state (corresponds to a specific range of H_s and T_e) are shown in purple numbers (hours/year) in the grids. The annual wave power contributed by each sea state is shown by the colors. Wave power in terms of H_s and T_e based on Eq. (1) is represented by the dashed lines. In regions open to the Southern Ocean (Fig. 14a–c, h-l), the maximum annual wave power storage corresponds to H_s of 2–5 m and T_e of 7–11 s. Note that the maximum joint occurrence of H_s and T_e does not guarantee maximum annual wave power production, because annual wave power is jointly controlled by the annual occurrence (unit: hours/year) and corresponding wave power produced per hour. For example, storms generally have high instantaneous wave power but with a relatively low occurrence in each year, which makes a relatively small contribution to the annual wave power. In regions protected by Tasmania (Fig. 14e–g, m-n), the maximum annual wave power storage is associated with H_s of 1–2.75 m and T_e of 4–7 s. Interestingly, the bivariate probability at TAS5-6 (Fig. 14m-n) has a tail that shows very long T_e and a low H_s.

In practice, the deployment of WECs is dependent on water depth, distance to the coast, urban regions, etc. Furthermore, electricity generation varies for different WECs, being a function of wave climate (e.g., H_s, T_e, D_p, and extreme waves). Some WECs (e.g., Pelamis) are designed to align their direction to the highest wave power [8], and other WECs (e.g., Wave Dragon) cannot take advantage of wave power from all

directions [17]. In this study, we assume that all the specific locations selected are suitable for installing a range of different WEC devices. The annual electric power (P_E) produced by 9 typical WECs (Seabased AB, Aqua Buoy, Wavebob, Langlee, Pelamis, Oceantec, OE Buoy, Pontoon, Wave Dragon) was calculated for each location based on the following equation [8,16],

$$P_E = \sum_{i=1}^{n_T} \sum_{j=1}^{n_{H_s}} p_{ij} P_{ij}, \qquad (14)$$

where p_{ij} is the occurrence percentage for a specific H_s and T_e, P_{ij} is the WEC power matrix that is available from Diaconu and Rusu [45].

The expected annual electric power produced at each location by the different WECs is shown in Fig. 15. The WEC power matrix (P_{ij}) of each device varies [45], which introduces the scale differences in Fig. 15. However, it does not mean that one WEC is necessarily superior to another (Fig. 15). For instance, the unit price of the Aqua Buoy is much lower than the Wave Dragon [46]. The results in Fig. 15 clearly show that different WEC units have a range of capabilities in producing electricity. However, all the WECs are expected to generate a significant amount of electricity at the locations open to the Southern Ocean (SA, VIC1-2, KI, TAS1-4), whilst WECs at the protected locations (VIC4-5, NSW, TAS5-6), not surprisingly, produce much less electric power, although the wave climate is more stable. The annual electric power across all the WECs shows that VIC1-2, KI, TAS1-3 have the most promising capacity for producing electricity, with TAS2 producing the largest output of the 14 locations (Fig. 15). VIC4-5 and TAS6 have the
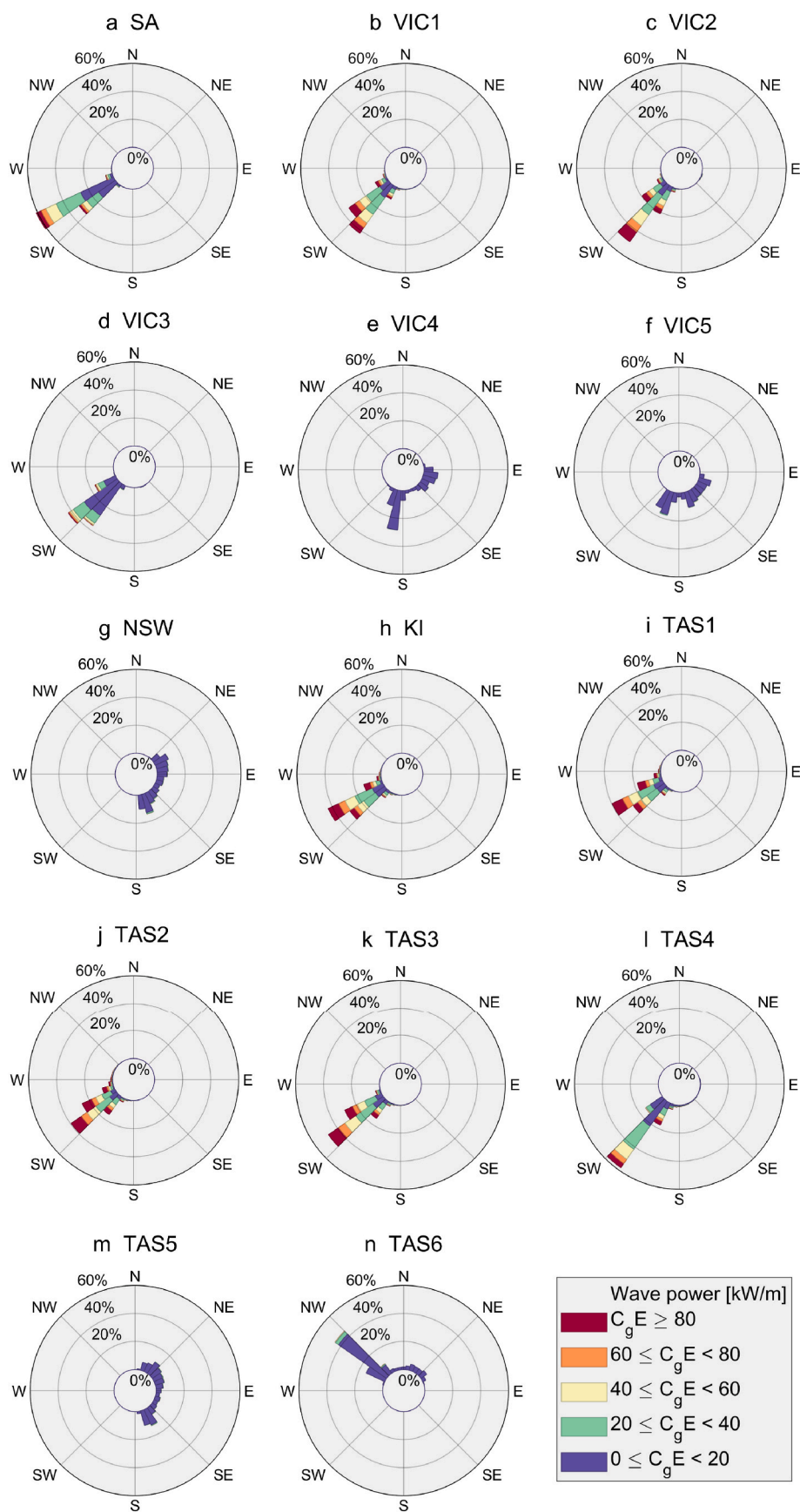
Fig. 12. Wave power roses at the selected locations shown in Fig. 10. The direction convention used is "waves coming from".
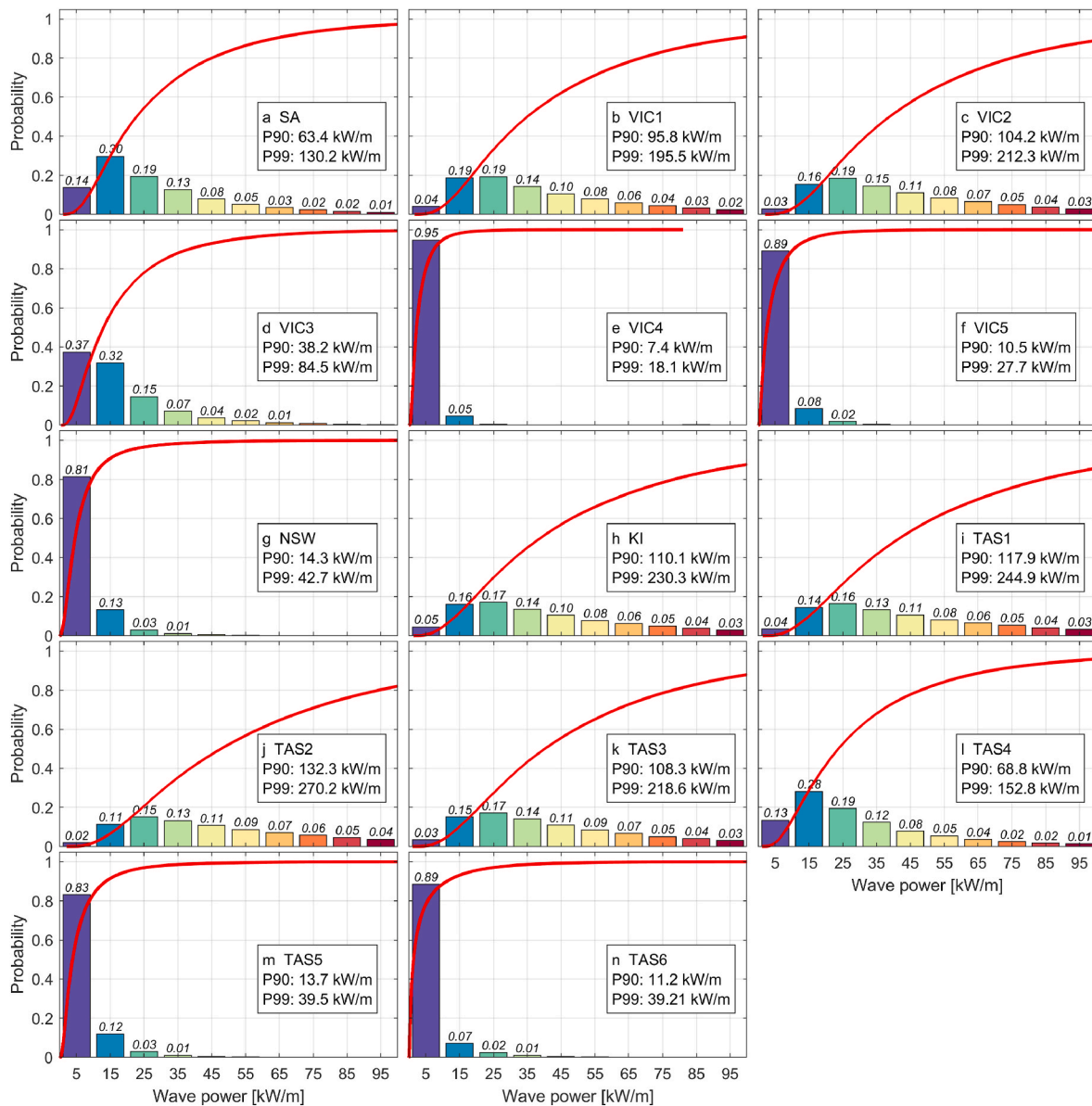
Fig. 13. Probability distribution of annual mean wave power at the selected locations shown in Fig. 10. The corresponding probability values are shown on the top of each bar. The location, 90th percentile (P90), and 99th percentile (P99) wave power are shown on each panel. The red lines mark cumulative probability distributions of annual mean wave power.

lowest potential for generating electric power (Fig. 15). Although their seasonal variations of wave power are relatively small (Fig. 11), mean wave power at these locations is too low to extract significant electrical power (Table 1). These results are comparable to the electric power estimations along the New South Wales of Morim et al. [8]. Note, however, that the locations considered by the two studies do not overlap.

Different WECs have distinct optimal environments for maximizing their electricity generation. Table 2 presents the key characteristics of these WECs, highlighting their typical installation in water depths greater than 20 m. Moreover, the feasible environments for WECs encompass onshore, near-shore, and offshore regions. Additionally, WECs vary in size and deployment expense.

One example of a WEC is Langlee, which is a semi-submersible oscillating wave surge converter utilizing water wings to harness wave motion. Another WEC, Wave Dragon, is a large overtopping device. Point absorber WECs, such as seabased AB, Aqua Buoy, Wavebob, Oceantec, OE Buoy, and Pontoon, generate electricity by exploiting the

relative movement between fixed and unfixed WEC structures. There are a range of distinguishing characteristics among these point absorbers. For instance, seabased AB, situated on the seabed, is designed to generate electricity underwater with minimal maintenance requirements and remains invisible. On the other hand, Wavebob generates electricity through the lifting or falling of ocean waves, even under complex wave conditions.

Considering the water depths specified in Table 2 and the selected locations outlined in Table 1, VIC4 is unsuitable for WEC installation due to its shallow water depth and low electricity generation. However, the remaining locations can accommodate one or multiple WECs, especially the selected locations of South Australia, western part of Victoria and southwestern part of Tasmania. VIC2, KI, and TAS1-3 are particularly promising for installing Aqua Buoy, Wavebob, and Pelamis WECs, respectively.

There are numerous factors that need to be considered when deploying WECs, particularly with regards to environmental concerns in coastal regions. One such concern is the potential alteration of
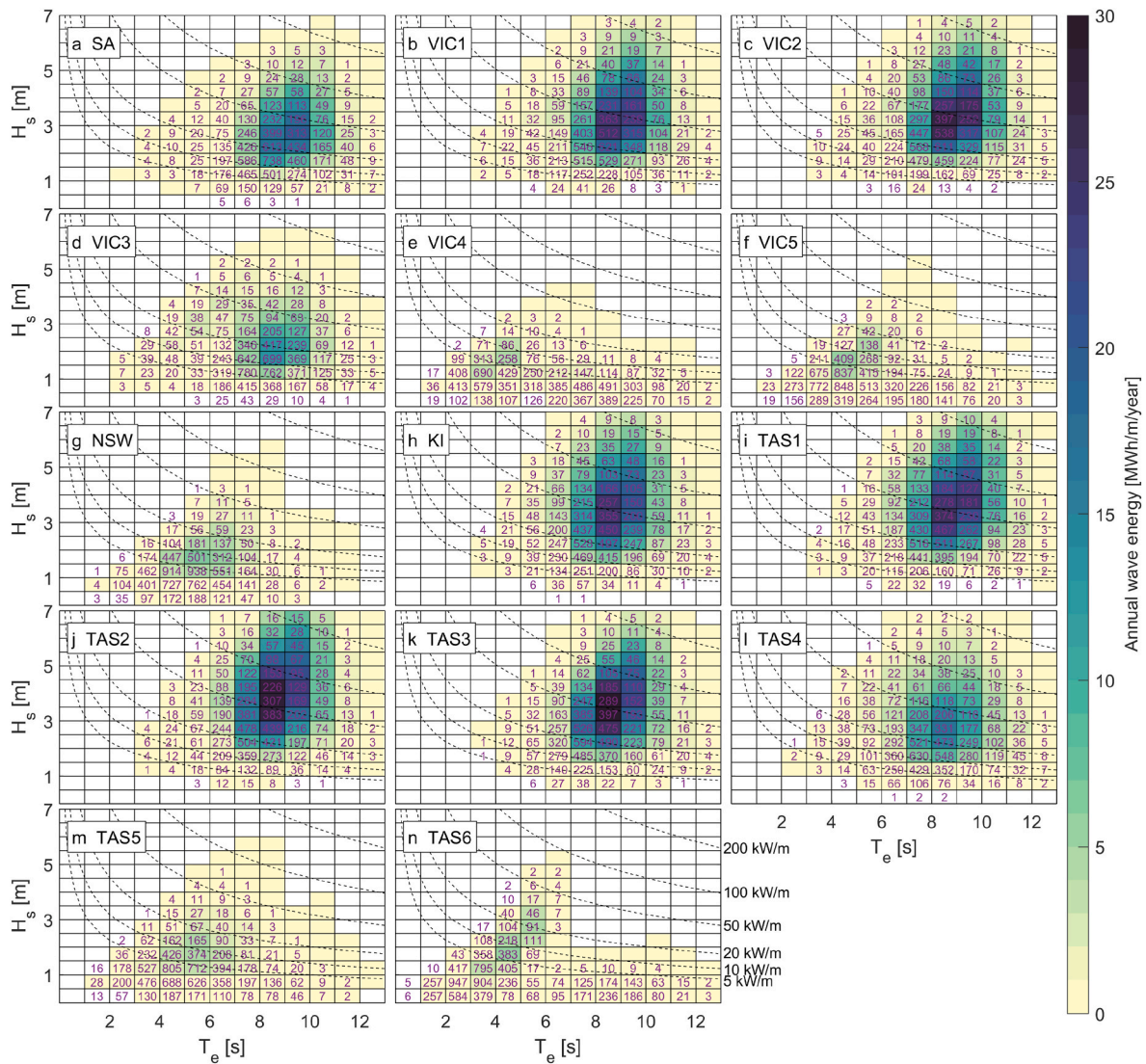
Fig. 14. Bivariate probability distribution of occurrence and annual wave energy at the selected locations. The numbers and colored grids represent annual occurrence (units: hours/year) and wave energy storage (MWh/m/year) for specific significant wave height (H_s) and energy period (T_e), respectively. The Eq (1)-based contour lines of wave power are shown in each panel and the labels are shown in the last panel.

electromagnetic fields and disruption of marine animal habitats due to the installation of WECs and electrical cables. Additionally, the deployment of WECs can impact long-shore sediment transport and result in sand accumulation. Economic feasibility is also a crucial factor that needs consideration. For instance, it is crucial to take into account the efficiency of wave power transmission and consumption from the WEC site to the onshore electricity receiver. Various factors, including cable losses, distance, and voltage conversion, must be considered to ensure the optimal transmission of power and minimize energy consumption. Moreover, WECs must be capable of withstanding corrosive saltwater and storms to ensure their longevity and cost-effectiveness. While offshore WECs have the potential to generate large amounts of electricity, they face the challenge of withstanding extreme wave conditions and require expensive maintenance [2]. On the other hand, WECs in nearshore regions may be more manageable and less costly to maintain, but they can potentially cause greater impacts on coastal communities.

5. Conclusions

With the increasing desire to develop renewable energy sources,

ocean wave energy has the potential to make an important contribution to sustainable development. Compared to wind and solar energy, wave energy is relatively reliable with less variability. The southern coast of Australia is exposed to the year-round energetic wave climate of the Southern Ocean. As such, it represents a promising region for wave energy development. This study used a high-resolution WW3 hindcast model dataset to investigate wave energy variability of south-east Australia over the period 1981–2020. The model results were extensively validated against a coastal buoy network by Liu et al. [10]. This study further verified the model outputs against measured H_s from 14 satellite altimeters and wave power derived from the altimeters. Both H_s and wave power hindcast by the model agree well with the altimeters across the full computational domain (Figs. 3 and 4).

Mean conditions (Fig. 5), seasonality (Fig. 6), and extreme values (Fig. 8) of wave power across the domain are impacted by Southern Ocean swell and the protection provided by Tasmania. The wave power is largest in the western and southern parts of the domain and smallest in Bass Strait and coastal regions of eastern Victoria. Seasonal wave power reaches a maximum (minimum) in winter (summer). The results show that H_s has its maximum contribution to the wave power in winter and T_p has its maximum contribution in summer in the southwestern
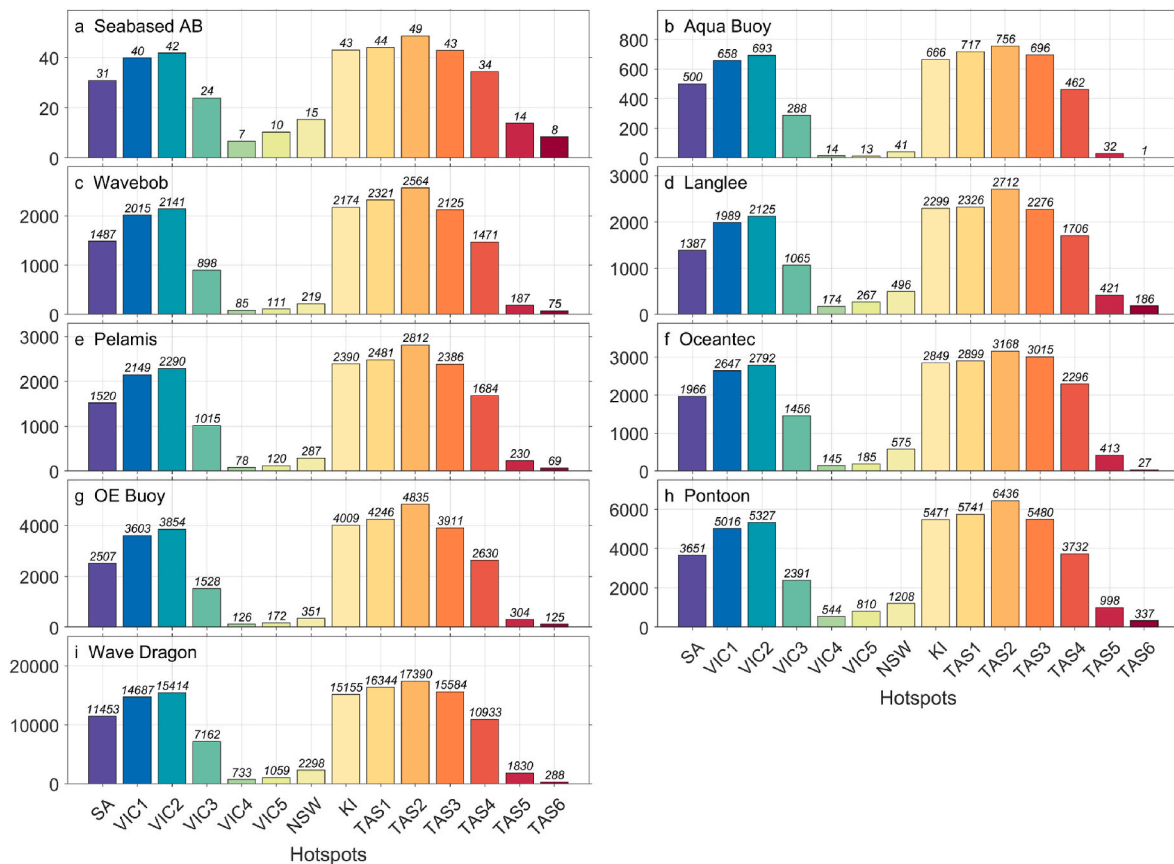
Fig. 15. Expected annual electric power (units: MWh) produced by different WECs at the selected locations. Noting the different scales of the y-axis (sorting the y-axis maxima in ascending order). The WEC names are shown on the upper left corner of each panel. The annual electric power at each location is marked at the top of each bar.

Table 2
WEC features [47,48].

WECs	Classification	Installation depth	Size
Seabased AB	Point absorber	30–50	Small
Aqua Buoy	Point absorber	50–60	Small
Wavebob	Point absorber	>50	Medium
Langlee	Oscillating surge transducer	Offshore	Medium
Pelamis	Attenuator	50–70	Medium
Oceantec	Point absorber	50–100	Medium
OE Buoy	Point absorber	>100	Medium
Pontoon	Point absorber	>100	Large
Wave Dragon	Overtopping terminator	>20	Large

proportion of the domain. The peak wave period, T_p makes the greatest contribution to wave power in the more protected central and eastern regions of the model domain (Fig. 6). Long-term trend analysis of wave power in the domain shows that increases in wave power over the 40 years are dominated by increases in H_s with the largest increases in the southeastern part of the model domain (Fig. 9).

A total of 14 locations (across South Australia, Victoria, New South Wales, King Island, and Tasmania) along the southeastern Australian coast were selected for detailed study of their wave power. The wave power in the western and southern parts of the domain is dominated by energetic southwesterly swell from the Southern Ocean. There is, however, considerable seasonal variability in the wave power climate of these exposed sites. (Fig. 11). The directions of waves are, however, relatively consistent (Fig. 12). In contrast, the wave climate in regions protected by Tasmania (nearshore regions of eastern Victoria) is dominated by the local climate system. Wave power at the selected locations in these regions is less energetic with waves coming from a broad range

of directions (northeasterly to southwesterly, Fig. 12). A total of 9 typical WECs were selected to estimate the electricity production at the selected locations (Fig. 15), which further confirms the potential for the Southern Ocean swell to contribute to electricity production. The exposed locations, VIC1-2, KI, and TAS1-3, not surprisingly show the greatest capacity for generating electricity regardless of the WEC type. VIC4-5 and TAS6 have the least potential as electricity production sites.

The present study focuses on the wave energy variability of southeast Australia based on a 40-year hindcast, which indicates the impacts of the Southern Ocean wave climate. Under plausible climate change scenarios, Southern Ocean swell is projected to be more energetic by 2100 due to the intensification of westerly winds [49,50]. Therefore, the southwestern part of the domain (e.g., western portion of Victoria and southern/western parts of Tasmania) is expected to experience an increase in wave climate [38,44]. However, H_s in nearshore regions of eastern Victoria and southern New South Wales is projected to be lower as local winds decrease by the end of the 21st century [38,44]. These variations will certainly change wave energy in the domain, which may impact WEC deployment in the coastal locations.

CRediT authorship contribution statement

Jin Liu: Conceptualization, Methodology, Software, Formal analysis, Data curation, Visualization, Writing – original draft, Writing – review &

editing. **Alberto Meucci:** Writing – review & editing. **Qingxiang Liu:** Writing – review & editing. **Alexander V. Babanin:** Writing – review & editing. **Daniel Ierodiaconou:** Funding acquisition, Writing – review & editing. **Xingkun Xu:** Writing – review & editing. **Ian R. Young:** Resources, Conceptualization, Methodology, Data curation, Supervision, Project administration, Funding acquisition, Writing – review & editing.

Declaration of competing interest

The authors declare that they have no known competing financial interests or personal relationships that could have appeared to influence the work reported in this paper.

Data availability

Data will be made available on request.

Acknowledgments

References

[1] E.D. Stoutenburg, N. Jenkins, M.Z. Jacobson, Power output variations of co-located offshore wind turbines and wave energy converters in California, Renew. Energy 35 (12) (2010) 2781–2791, https://doi.org/10.1016/j.renene.2010.04.033.

[2] I. López, J. Andreu, S. Ceballos, I.M. De Alegría, I. Kortabarria, Review of wave energy technologies and the necessary power-equipment, Renew. Sustain. Energy Rev. 27 (2013) 413–434, https://doi.org/10.1016/j.rser.2013.07.009.

[3] J. Morim, N. Cartwright, A. Etemad-Shahidi, D. Strauss, M. Hemer, A review of wave energy estimates for nearshore shelf waters off Australia, Int. J. Mar. Energy 7 (2014) 57–70, https://doi.org/10.1016/j.ijome.2014.09.002.

[4] I.R. Young, E. Fontaine, Q. Liu, A.V. Babanin, The wave climate of the Southern Ocean, J. Phys. Oceanogr. 50 (5) (2020) 1417–1433, https://doi.org/10.1175/JPO-D-20-0031.1.

[5] M. Hemer, D. Griffin, The wave energy resource along Australia's Southern margin, J. Renew. Sustain. Energy 2 (4) (2010) 043108, https://doi.org/10.1063/1.3464753.

[6] M.G. Hughes, A.D. Heap, National-scale wave energy resource assessment for Australia, Renew. Energy 35 (8) (2010) 1783–1791, https://doi.org/10.1016/j.renene.2009.11.001.

[7] M.V. Cuttler, J.E. Hansen, R.J. Lowe, Seasonal and interannual variability of the wave climate at a wave energy hotspot off the southwestern coast of Australia, Renew. Energy 146 (2020) 2337–2350, https://doi.org/10.1016/j.renene.2019.08.058.

[8] J. Morim, N. Cartwright, A. Etemad-Shahidi, D. Strauss, M. Hemer, Wave energy resource assessment along the Southeast coast of Australia on the basis of a 31-year hindcast, Appl. Energy 184 (2016) 276–297, https://doi.org/10.1016/j.apenergy.2016.09.064.

[9] F. Flocard, D. Ierodiaconou, I.R. Coghlan, Multi-criteria evaluation of wave energy projects on the south-east Australian coast, Renew. Energy 99 (2016) 80–94, https://doi.org/10.1016/j.renene.2016.06.036.

[10] J. Liu, A. Meucci, Q. Liu, A.V. Babanin, D. Ierodiaconou, I.R. Young, The wave climate of Bass Strait and south-east Australia, Ocean Model. 172 (2022) 101980, https://doi.org/10.1016/j.ocemod.2022.101980.

[11] J. Liu, J. Dai, D. Xu, J. Wang, Y. Yuan, Seasonal and interannual variability in coastal circulations in the northern South China Sea, Water 10 (4) (2018) 520, https://doi.org/10.3390/w10040520.

[12] A. Ribal, I.R. Young, 33 years of globally calibrated wave height and wind speed data based on altimeter observations, Sci. Data 6 (1) (2019) 1–15, https://doi.org/10.1038/s41597-019-0083-9.

[13] WW3DG, User Manual and System Documentation of WAVEWATCH III Version 6.07, NOAA/NWS/NCEP/MMAB, 2019.

[14] A. Ribal, A.V. Babanin, S. Zieger, Q. Liu, A high-resolution wave energy resource assessment of Indonesia, Energy 160 (2020) 1349–1363, https://doi.org/10.1016/j.renene.2020.06.017.

[15] A. Akpinar, B. Bingölbali, G.P. Van Vledder, Long-term analysis of wave power potential in the Black Sea, based on 31-year SWAN simulations, Ocean Eng. 130 (2017) 482–497, https://doi.org/10.1016/j.oceaneng.2016.12.023.

[16] M. Gonçalves, P. Martinho, C.G. Soares, Wave energy assessment based on a 33-year hindcast for the Canary Islands, Renew. Energy 152 (2020) 259–269, https://doi.org/10.1016/j.renene.2020.01.011.

[17] Y. Lin, S. Dong, Z. Wang, C.G. Soares, Wave energy assessment in the China adjacent seas on the basis of a 20-year SWAN simulation with unstructured grids, Renew. Energy 136 (2019) 275–295, https://doi.org/10.1016/j.renene.2019.01.011.

[18] B.G. Reguero, I.J. Losada, F.J. Méndez, A recent increase in global wave power as a consequence of oceanic warming, Nat. Commun. 10 (1) (2019) 1–14, https://doi.org/10.1038/s41467-018-08066-0.

[19] Cornett AM. A Global Wave Energy Resource Assessment. Conference A Global Wave Energy Resource Assessment. International Society of Offshore and Polar Engineers.

[20] W.-R. Su, H. Chen, W.-B. Chen, C.-H. Chang, L.-Y. Lin, J.-H. Jang, et al., Numerical investigation of wave energy resources and hotspots in the surrounding waters of Taiwan, Renew. Energy 118 (2018) 814–824, https://doi.org/10.1016/j.renene.2017.11.080.

[21] H.-J. Shih, C.-H. Chang, W.-B. Chen, L.-Y. Lin, Identifying the optimal offshore areas for wave energy converter deployments in Taiwanese waters based on 12-year model hindcasts, Energies 11 (3) (2018) 499, https://doi.org/10.3390/en11030499.

[22] Z. Sun, H. Zhang, D. Xu, X. Liu, J. Ding, Assessment of wave power in the South China Sea based on 26-year high-resolution hindcast data, Energy 197 (2020), 117218, https://doi.org/10.1016/j.energy.2020.117218.

[23] C. Gommenginger, M. Srokosz, P. Challenor, P. Cotton, Measuring ocean wave period with satellite altimeters: a simple empirical model, Geophys. Res. Lett. 30 (22) (2003), https://doi.org/10.1029/2003GL017743.

[24] H.L. Tolman, A third-generation model for wind waves on slowly varying, unsteady, and inhomogeneous depths and currents, J. Phys. Oceanogr. 21 (6) (1991) 782–797, https://doi.org/10.1175/1520-0485(1991)021<0782:atgmfw>2.0.co;2.

[25] H.L. Tolman, Effects of numerics on the physics in a third-generation wind-wave model, J. Phys. Oceanogr. 22 (10) (1992) 1095–1111, https://doi.org/10.1175/1520-0485(1992)022<1095:eonotp>2.0.co;2.

[26] L. Cavaleri, P.M. Rizzoli, Wind wave prediction in shallow water: theory and applications, J. Geophys. Res. Oceans 86 (C11) (1981) 10961–10973, https://doi.org/10.1029/jc086ic11p10961.

[27] S. Hasselmann, K. Hasselmann, J. Allender, T. Barnett, Computations and parameterizations of the nonlinear energy transfer in a gravity-wave specturm. Part II: parameterizations of the nonlinear energy transfer for application in wave models, J. Phys. Oceanogr. 15 (11) (1985) 1378–1391, https://doi.org/10.1175/1520-0485(1985)015<1378:capotn>2.0.co;2.

[28] S.-C. Hsiao, H.-L. Wu, W.-B. Chen, Study of the optimal grid resolution and effect of wave–wave interaction during simulation of extreme waves induced by three ensuing typhoons, J. Mar. Sci. Eng. 11 (3) (2023) 653, https://doi.org/10.3390/jmse11030653.

[29] K. Hasselmann, T.P. Barnett, E. Bouws, H. Carlson, D.E. Cartwright, K. Enke, et al., Measurements of wind-wave growth and swell decay during the Joint North Sea Wave Project, JONSWAP, 1973. Ergänzungsheft.

[30] Battjes JA, Janssen J. Energy loss and set-up due to breaking of random waves. Coast. Eng. 19781978. p. 569-587.

[31] W.E. Rogers, A.V. Babanin, D.W. Wang, Observation-consistent input and whitecapping dissipation in a model for wind-generated surface waves: description and simple calculations, J. Atmos. Ocean Sci. 29 (9) (2012) 1329–1346, https://doi.org/10.1175/jtech-d-11-00092.1.

[32] S. Zieger, A.V. Babanin, W.E. Rogers, I.R. Young, Observation-based source terms in the third-generation wave model WAVEWATCH, Ocean Model. 96 (2015) 2–25, https://doi.org/10.1016/j.ocemod.2015.07.014.

[33] K.J. Roberts, W.J. Pringle, J. Westerink, OceanMesh2D 1.0: MATLAB-based software for two-dimensional unstructured mesh generation in coastal ocean modeling, Geosci. Model Dev. (GMD) 12 (5) (2019) 1847–1868, https://doi.org/10.5194/gmd-12-1847-2019.

[34] S.-C. Hsiao, C.-T. Cheng, T.-Y. Chang, W.-B. Chen, H.-L. Wu, J.-H. Jang, et al., Assessment of offshore wave energy resources in Taiwan using long-term dynamically downscaled winds from a third-generation reanalysis product, Energies 14 (3) (2021) 653, https://doi.org/10.3390/en14030653.

[35] H. Hersbach, B. Bell, P. Berrisford, S. Hirahara, A. Horányi, J. Muñoz-Sabater, et al., The ERA5 global reanalysis, Q. J. R. Meteorol. Soc. 146 (730) (2020) 1999–2049, https://doi.org/10.1002/qj.3803.

[36] Q. Liu, A.V. Babanin, W.E. Rogers, S. Zieger, I.R. Young, J.-R. Bidlot, et al., Global wave hindcasts using the observation-based source terms: description and validation, J. Adv. Model. Earth Syst. 13 (8) (2021), https://doi.org/10.1029/2021MS002493.

[37] S. Kaur, P. Kumar, E. Weller, I.R. Young, Positive relationship between seasonal Indo-Pacific Ocean wave power and SST, Sci. Rep. 11 (1) (2021) 1–9, https://doi.org/10.1038/s41598-021-97047-3.

[38] J. Liu, A. Meucci, I.R. Young, Projected 21st century wind-wave climate of Bass Strait and south-east Australia: comparison of EC-Earth3 and ACCESS-CM2 climate model forcing, J. Geophys. Res. Oceans 128 (4) (2023), e2022JC018996, https://doi.org/10.1029/2022JC018996.

[39] R. McCarroll, G. Masselink, M. Wiggins, T. Scott, O. Billson, D. Conley, et al., High-efficiency gravel longshore sediment transport and headland bypassing over an extreme wave event, Earth Surf. Process. Landforms 44 (13) (2019) 2720–2727, https://doi.org/10.1002/esp.4692.

[40] M. Wiggins, T. Scott, G. Masselink, P. Russell, N.G. Valiente, Regionally-coherent embayment rotation: behavioural response to bi-directional waves and atmospheric forcing, J. Mar. Sci. Eng. 7 (4) (2019) 116, https://doi.org/10.3390/jmse7040116.

[41] C. Leach, D. Kennedy, N. Pucino, S. Doumtsis, K. Sorrell, B. Allan, et al., Measuring drivers of shoreline and subaerial beach change using limited datasets in a temperate, wave-dominated sandy system: Inverloch, Australia, Ocean Coast Manag. 240 (2023), 106641, https://doi.org/10.1016/j.ocecoaman.2023.106641.

[42] H. Rapizo, T.H. Durrant, A.V. Babanin, An assessment of the impact of surface currents on wave modeling in the Southern Ocean, Ocean Dynam. 68 (8) (2018) 939–955, https://doi.org/10.1007/s10236-018-1171-7.

[43] G.J. Marshall, Trends in the Southern Annular Mode from observations and reanalyses, J. Clim. 16 (24) (2003) 4134–4143, https://doi.org/10.1175/1520-0442(2003)016<4134:titsam>2.0.co;2.

[44] J. Liu, A. Meucci, I.R. Young, Projected wave climate of Bass Strait and south-east Australia by the end of the twenty-first century, Clim. Dynam. 60 (2022) 393–407, https://doi.org/10.1007/s00382-022-06310-4.

[45] Diaconu S, Rusu E. Evaluation of various WEC devices in the Romanian near shore. WSEAS International Conference on Energy and Environment Technologies and Equipment (EEETE'13), Brasov, Romania.

[46] E. Rusu, F. Onea, A review of the technologies for wave energy extraction, Clean Energy 2 (1) (2018) 10–19, https://doi.org/10.1093/ce/zky003.

[47] A.G. Majidi, B. Bingölbali, A. Akpınar, E. Rusu, Wave power performance of wave energy converters at high-energy areas of a semi-enclosed sea, Energy 220 (2021), 119705, https://doi.org/10.1016/j.energy.2020.119705.

[48] E. Rusu, Evaluation of the wave energy conversion efficiency in various coastal environments, Energies 7 (6) (2014) 4002–4018, https://doi.org/10.3390/en7064002.

[49] M.A. Hemer, Y. Fan, N. Mori, A. Semedo, X.L. Wang, Projected changes in wave climate from a multi-model ensemble, Nat. Clim. Change 3 (5) (2013) 471–476, https://doi.org/10.1038/NCLIMATE1791.

[50] J. Morim, M. Hemer, X.L. Wang, N. Cartwright, C. Trenham, A. Semedo, et al., Robustness and uncertainties in global multivariate wind-wave climate projections, Nat. Clim. Change 9 (9) (2019) 711–718, https://doi.org/10.1038/s41558-019-0542-5.